γ-ray cascade transitions in ^{112}Cd and ^{114}Cd following resonance capture of epithermal neutrons

G. Rusev, M. Jandel, M. Krtička, T. A. Bredeweg, A. Couture, T. N. Taddeucci, and J. L. Ullmann

Phys. Rev. C **87**, 054603 — Published 3 May 2013

DOI: 10.1103/PhysRevC.87.054603

Gamma-ray cascade transitions in ^{112}Cd and ^{114}Cd following resonance capture of epithermal neutrons

G. Rusev,[1] M. Jandel,[1] M. Krtička,[2] T. A. Bredeweg,[1] A. Couture,[3] T. N. Taddeucci,[3] and J. L. Ullmann[3]

[1] *Chemistry Division, Los Alamos National Laboratory, Los Alamos, New Mexico 87545, USA*
[2] *Faculty of Mathematics and Physics, Charles University, 18000 Prague 8, Czech Republic*
[3] *Los Alamos Neutron Science Center, Los Alamos National Laboratory, Los Alamos, New Mexico 87545, USA*

(Dated: April 8, 2013)

Cascades of γ-ray transitions in ^{112}Cd and ^{114}Cd have been studied in a neutron-capture experiment at the Los Alamos Neutron Science Center using a highly-segmented and highly-efficient γ-ray calorimeter - Detector for Advanced Neutron Capture Experiments. Intensity distributions of two-, three-, and multi-fold coincidence γ-ray transitions de-exciting resonances with known angular momenta and terminating at the ground state and at the first excited levels have been obtained. The results are compared with statistical-model calculations using the code `DICEBOX` for the two theoretical models of electric-dipole photon-strength functions, the Standard Lorentzian and the model of Kadmenskii, Markushev and Furman. It has been found that a combination of the two models reproduces the data best. Adding resonance structures, such as the scissors mode and the pygmy resonance, to the photon-strength function do not improve the description of the γ-ray spectra.

PACS numbers: 24.10.Lx, 24.60.Dr, 25.40.Lw, 27.60.+j, 28.20.Np

I. INTRODUCTION

Modeling of the statistical γ-ray transitions plays an important role in nuclear-reaction theory. Interpreting the intensity distribution of these γ rays, in the framework of the statistical model, as a depending only on the photon strength function (PSF) and the density of the final levels [1] give us the opportunity for easy prediction of the γ-ray output from a given reaction. Nowadays, astrophysics network calculations and calculations regarding nuclear spent-fuel transmutation, based on the Hauser-Feschbach approach [2], demand reliable PSF models in order to extend the calculations to nuclei away from the valley of stability.

The shape of the PSF for $E1$ transitions is established from (γ, n) measurements at γ-ray energies (E_γ) above the neutron-separation energy (S_n) and can be reasonably described via a Lorentzian shape of the Giant Dipole Resonance (GDR), while at $E_\gamma < S_n$ it is not understood well. Extrapolation of the GDR to energies below S_n, which gives the average probability for an $E1$ excitation and thus the $E1$ PSF, becomes difficult because of the scarce data on the photoabsorption cross sections at low energies. The PSF at these energies can be deduced from other sources. The two dominant sources are neutron-capture and ^{3}He-induced reactions. Unfortunately, noticeable discrepancies in the PSFs deduced from the three techniques prevent us of having a common description of the γ-ray output of any reaction at the moment. Photon-induced experiments suggested the Lorentzian curve as a GDR extrapolation down to 4-5 MeV for several nuclei [3–6], but considering the Lorentzian curve as the shape of the $E1$ PSF provides a larger total radiative width at S_n than the measured one from neutron resonances [4]. In addition, the PSFs deduced from neutron-capture and ^{3}He-induced experiments indicate a γ-ray energy dependence which is different from the Lorentzian shape, but rather very similar to the model of Kadmenskii, Markushev and Furman. In some cases even these two types of reactions, (n, γ) and (^{3}He,^{3}He$'\gamma$) or (^{3}He,$\alpha\gamma$), are in disagreement [7]. As a result, the available experimental data is still challenging to explain fully the de-excitation γ-ray spectra from particle-induced reactions by the known photo-excitation modes in the nucleus.

The electromagnetic properties of the nucleus are directly measured with photon-induced reactions. An important question is to what extent structures observed in photon-scattering experiments, such as "scissors mode" and "pygmy" dipole resonances, influence the γ-ray cascade transitions from particle-induced reactions. It has been observed in neutron-capture [8] and ^{3}He-scattering [9, 10] experiments that the low-energy $M1$ excitations in deformed nuclei (the scissors mode resonance) known previously from photon- and electron-scattering experiments [11] are needed to reproduce the γ-ray cascades correctly. The pygmy dipole resonance (PDR) is an $E1$ excitation mode superimposed on the GDR tail at energies below or around S_n. A bump at 5.5 MeV observed in previous (n, γ) experiments on a few heavy isotopes has been associated with PDR [1], but it has not been proved to be a generic mode of de-excitation existing in all nuclei and following the Brink hypothesis [12], i.e. PDR to be built on excited states. Furthermore, a photon-scattering experiment on ^{142}Nd [13] suggested that at least a fraction of the PDR does not follow the Brink hypothesis. Inelastic ^{3}He-scattering experiments indicate an increase of the strength in the PDR region [14, 15], but do not provide a clear resonance-like PDR structure.

The neutron-capture reaction is very suitable for investigation of the statistical γ-ray transitions because, in general, the neutron resonances are weakly coupled to the ground state or the first excited levels providing many-fold cascade transitions. Also, γ-ray spectra from isolated resonances with known angular momenta

can be selected using the time-of-flight technique and the sum energy of the γ rays of each cascade measured if a calorimeter is used providing information for the starting and terminating levels of the γ-ray cascades. Although, the multi-detector array systems used in neutron-capture experiments allow a measurement of two-, three- and multi-fold coincidence γ rays, the shape of spectra of low-multiplicity cascades remain the most sensitive ones to the PSF. An additional quantity relevant to the PSF determination is the multiplicity distribution of the γ-ray cascade transitions, representing the distribution of the number of cascades for each multiplicity.

In the present work, we focus on the investigation of the PSF describing the γ-ray cascade transitions in ^{112}Cd and ^{114}Cd. The cadmium isotopes are well known with their vibrational properties [16, 17] which may influence the shape of PSF. In addition, an accurate description of the γ-ray intensity distribution following neutron capture from ^{111}Cd and ^{113}Cd is of importance for applications in building reliable neutron shielding or cadmium doped neutron detectors due to their large (n,γ) cross sections.

II. EXPERIMENTAL DETAILS

A neutron-capture experiment on natural cadmium has been performed for 47 hours at the Manuel J. Lujan, Jr. Neutron Scattering Center at the Los Alamos Neutron Science Center (LANSCE) [18]. Spallation neutrons produced by irradiation of a tungsten target with 800-MeV protons with a repetition rate of 20 Hz were used in the experiment. The low-energy part of the neutron-flux distribution was additionally enhanced by a water-moderator block with a thickness of 2.54 cm. The spallation target is shielded by a 2-m thick concrete wall. The neutrons are collimated to a narrow beam by a double-truncated copper collimator forming a spot at the target position with a full width at the half maximum of 0.7 cm. The collimator consists of four sections with a total length of 3 m. A detailed description of the neutron facility at the Lujan Center and the properties of the beam can be found in Refs. [19, 20].

A. Neutron-capture experiment on natural Cd

A sample of natural cadmium with thickness of 372 mg/cm^2 was positioned at the center of the Detector for Advanced Neutron Capture Experiments (DANCE) at a distance of 20.25 m from the spallation neutron source. DANCE is a high-granularity γ-ray calorimeter consisting of 160 BaF_2 crystals in a 4π geometry with an efficiency of 86% for a single photon with energy of 1 MeV [21]. A natural cadmium filter with a thickness of 2.46 g/cm^2 was placed between the first and second sections of the collimator to suppress the flux of thermal neutrons and thus to reduce the counting rate of DANCE.

E_0 (eV)	J	l	$2g\Gamma_n$ (meV)	Γ_γ (meV)
^{111}Cd(n,γ)				
99.4(4)	1	0	20(1)	92(14)
102.9(4)	1	0	1.6(2)	
138.1(6)	0	0	16(1)	96(12)
164.1(7)	1	0	97(10)	110(9)
225.1(9)	1	0	45(6)	
332(1)	1	0	9.5(7)	
357(1)	1	0	66(6)	98(15)
389(1)	1	0	40(11)	
478(1)	0	0	5.9(2)	
540(1)	[1]	0	35(1)	120(25)
604(1)	1	0	54(5)	104(18)
^{113}Cd(n,γ)				
63.70(2)	1	0	5.20(6)	90(20)
108.33(2)	1	0	17.04(12)	90(12)
143.07(3)	0	0	4.68(6)	
158.76(3)	1	0	12.94(12)	90(20)
192.85(4)	0	0	91.6(2)	110(20)
215.23(5)	1	0	40.4(2)	110(20)
261.07(6)	1	0	52.6(4)	110(15)
269.35(6)	0	0	35.0(2)	100(20)
291.61(6)	1	0	8.80(14)	
432.01(9)	1	0	36.6(4)	100(20)
501.0(1)	1	0	73.8(6)	100(20)
524.8(1)	1	0	52.2(6)	110(25)
551.9(1)	1	0	158.6(10)	110(20)
623.7(1)	1	0	30.8(4)	

TABLE I: Energies, spins, neutron and radiative widths of the s-wave resonances in the ^{111}Cd(n,γ) and ^{113}Cd(n,γ) reactions used in the analysis in the present work. All values are taken from the evaluation by S. F. Mughabghab [22].

The data acquisition of DANCE and the signal processing are described in more detail in Refs. [21, 23]. We will define only the quantities relevant to the current work extracted from the raw DANCE data in an off-line analysis. Because DANCE is a 4π array, the sum γ-ray energy, E_γ^{total}, of all detectors that fired within a coincidence window of 5 ns provides the energy of the neutron-capture level if there are no states with a lifetime longer than 5 ns in the measured γ-ray cascade. The sum energy equals to the Q-value of the (n,γ) reaction.

Often a γ ray may scatter from one BaF_2 crystal to a neighboring one and much more seldomly to a third crystal distributing its energy over two or more detectors creating a cluster of fired crystals. To obtain the correct energy of the incident γ ray we applied the add-back procedure [24] in the off-line analysis of the event-by-event data by adding the registered energy in each detector of the cluster. The sum energy of the detectors in the cluster we will consider as the energy E_γ of the detected γ ray. The number of the γ rays detected in one DANCE event gives the multiplicity, M_γ, of the γ-ray cascade.

A time-of-flight (TOF) spectrum converted to neutron energy ($t(\mu s) = 1464.1/\sqrt{E_n(\mathrm{eV})}$) is shown in Fig. 1. The spectrum was collected within a TOF interval from 0 to 500 μs (corresponding to $E_n > 8.57$ eV) after the proton bunch struck the spallation target and with an ad-

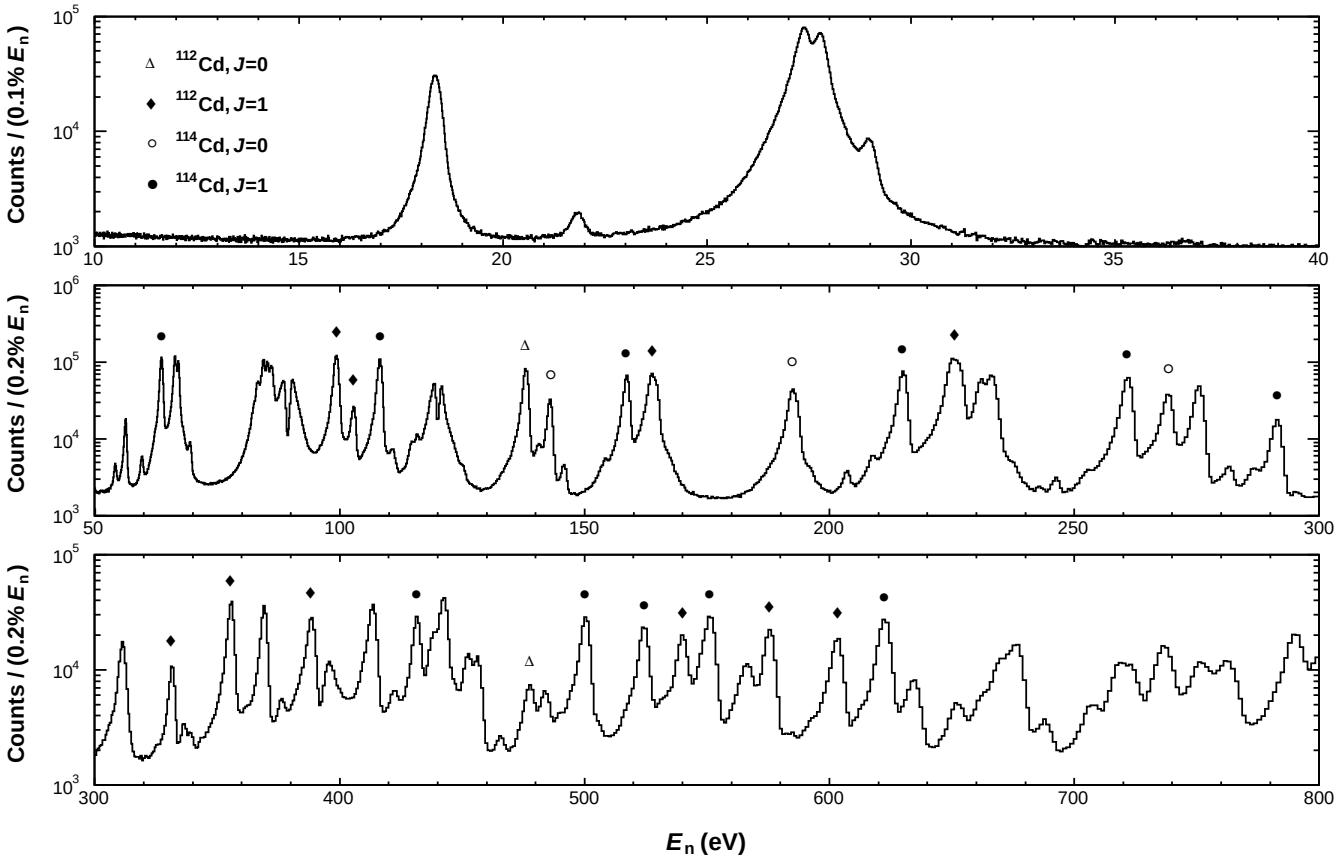

FIG. 1: Time-of-flight spectrum, converted to neutron energy, from $^{\rm nat}$Cd measured with DANCE. The events were collected under the condition that at least three γ rays were registered by the detector array in order to reduce the background. The s-wave resonances in the ^{111}Cd(n,γ) and ^{113}Cd(n,γ) reactions with known spins used in the analysis of the photon strength functions are denoted with figures. The properties of these resonances are listed in Table I.

ditional condition of at least three γ rays to be registered by DANCE in order to reduce the background due to elastic scattering of neutrons from the target, see below. Only well isolated s-wave resonances with known angular momenta in the TOF spectrum (cf. Fig. 1) were considered in the analysis of the cascade transitions following neutron capture from ^{111}Cd and ^{113}Cd. The energies, spins, neutron and radiative widths of those resonances, taken from the evaluation by S. F. Mughabghab [22], are listed in Table I.

B. Background due to elastic neutron scattering

The background in the measured spectra with DANCE have different components, for example, the ambient background of neutrons and γ rays penetrating the shielding of the proton-beam transport, scattered γ rays, which accompany the neutrons in the beam, from the target, and other. A detailed study of the background in (n,γ) measurements with DANCE is given in Ref. [25]. Some of the background contributions result in detection of low-energy γ rays with a sum energy much smaller than the Q values of the considered reactions ^{111}Cd(n,γ) and ^{113}Cd(n,γ). Their contributions can be easily removed in the off-line data analysis by requiring E_γ^{total} to equal the Q value of the reaction. Because we aim at measuring of the intensity and multiplicity distributions of the capture γ rays in the cadmium isotopes, a background which has a uniform distribution, for example the cosmic background below 10 MeV, can be ignored because it does not change the shape of the spectra.

The only background, which can affect our measurement is due to capture of neutrons by the barium isotopes in the BaF_2 crystals. These barium-capture γ rays will be superimposed on the spectra of interest from ^{112}Cd and ^{114}Cd leading to observation of additional peaks or structures. The major source of this background are the neutrons scattered from the target to the DANCE array. To reduce this "sample related" background, a shell of ^{6}LiH with thickness of 6 cm surrounds the target and captures most of the scattered neutrons via the ^{6}Li$(n,t)^4$He reaction without emission of γ rays. In addition, the neutron beam propagates in an evacuated pipe and is stopped in a beam dump to avoid scattering of the beam from the air to DANCE and room-return neutrons, respectively.

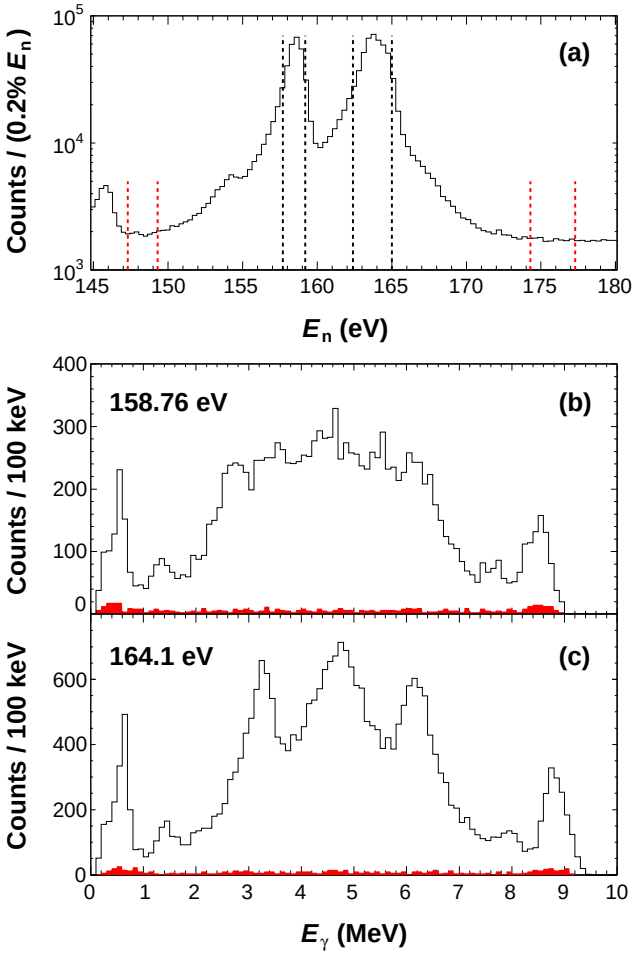

FIG. 2: (Color online) Part of the time-of-flight spectrum (a) with gating regions (vertical dashed lines) for the background and two resonances. The multiplicity 2 spectra from the resonances at 158.76 eV in ^{113}Cd(n,γ) (b) and 164.1 eV in ^{112}Cd(n,γ) (c) after sum-energy cuts for the corresponding reactions were applied (see text) are compared with the background. The background spectra shown in red were scaled to the width of the gate of each of the resonances.

In the analysis of the data, we require E_γ^{total} to be equal within a given interval to the Q value of the ^{111}Cd(n,γ) or ^{113}Cd(n,γ) reaction of 9.394 and 9.043 MeV, respectively. This E_γ^{total} cut removes the capture contributions from ^{130}Ba (Q = 7.494 MeV), ^{132}Ba (Q = 7.190 MeV), ^{134}Ba (Q = 6.972 MeV), ^{136}Ba (Q = 6.906 MeV) and ^{138}Ba (Q = 4.723 MeV). But we may expect a small contribution to the background resulting from neutron capture in the odd-mass isotopes ^{135}Ba (Q = 9.108 MeV) and ^{137}Ba (Q = 8.612 MeV) with natural abundances of 6.59% and 11.23%, respectively. A comparison shown in Fig. 2 of two-step cascade spectra gated on two of the cadmium resonances with the spectra gated on the background region proves that the background contribution is negligible and structureless. The small peaks seen at around 0.5 and 8.5 MeV in the background spectra in Fig.

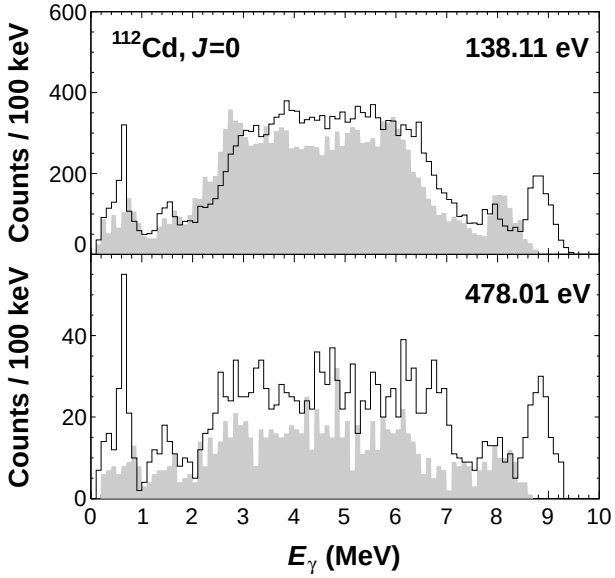

FIG. 3: Two-step cascade spectra from the J = 0 capture levels in ^{112}Cd. The resonance energy is given in the top-right corner of each plot. The filled gray histograms correspond to multiplicity 2 spectra in coincidence with the transition from the 2_1^+ level to the ground state at 620 keV. All spectra were collected under the requirement that the sum energy of all γ rays registered by DANCE is within the interval from 9.2 to 9.6 MeV representing the Q value of the ^{111}Cd$(n,\gamma)^{112}$Cd reaction of 9.394 MeV.

2 (b) and around 0.6 and 8.8 in Fig. 2 (c) are result of the contribution from neighboring cadmium resonances.

C. Cascade γ-ray spectra

Due to the high granularity of DANCE, spectra corresponding to two-, three- and many-fold γ-ray coincidences can be collected with a high efficiency. We will define them as multi-step cascade (MSC) spectra. The spectra have been sorted out from the raw event-by-event data using the FARE [26] software for DANCE-data analysis on a 56-core cluster computing system. The energy calibration for each detector was obtained from the peaks provided by ^{22}Na and ^{88}Y sources. The linearity of the calibration at high energies was verified by the position of the transition to the first excited state in the two-step cascade spectra. As discussed above, a gate on the sum energy of the γ rays detected with DANCE reduces the background. E_γ^{total} cuts from 9.2 to 9.6 MeV and from 8.8 to 9.2 MeV have been applied to the γ-ray spectra deexciting each of the considered the resonances in ^{112}Cd and ^{114}Cd, respectively. These narrow E_γ^{total} windows relative to the resolution of the BaF_2 detectors were required because of the close Q values for the ^{111}Cd(n,γ) and ^{113}Cd(n,γ) reactions of 9.394 and 9.043 MeV, respectively. Gamma-ray spectra were collected for each resonance listed in Table I by applying a neutron-energy

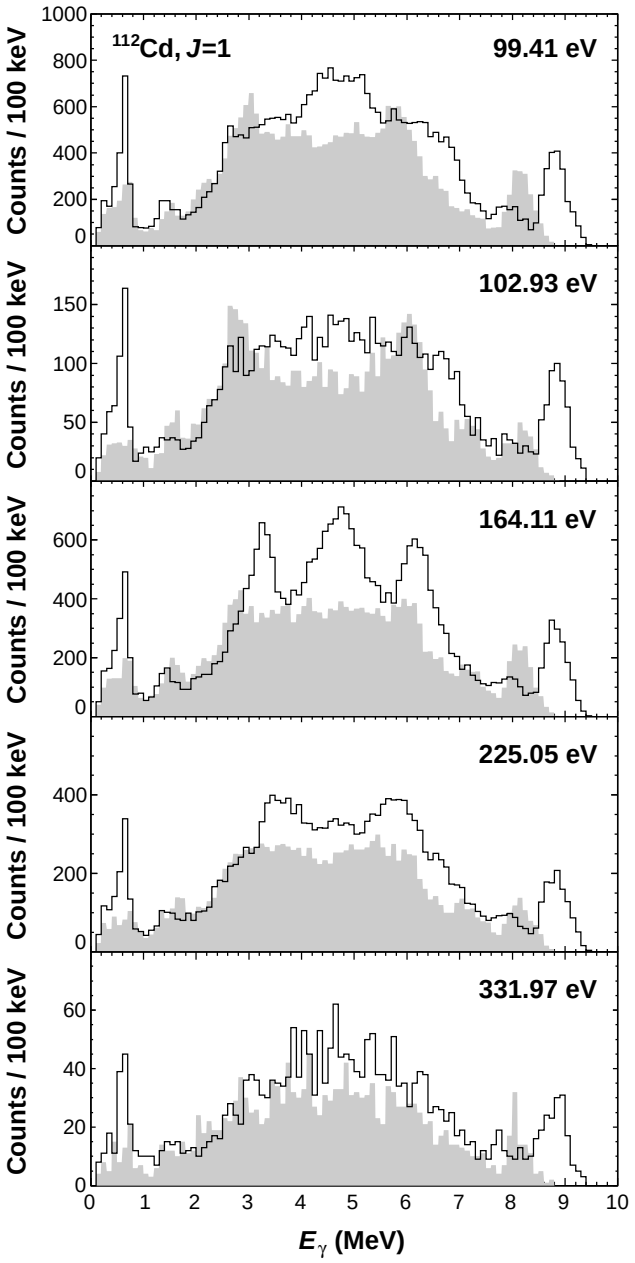

FIG. 4: Analogous to Fig. 3 but for the first five $J = 1$ capture resonances in ^{112}Cd in Table I.

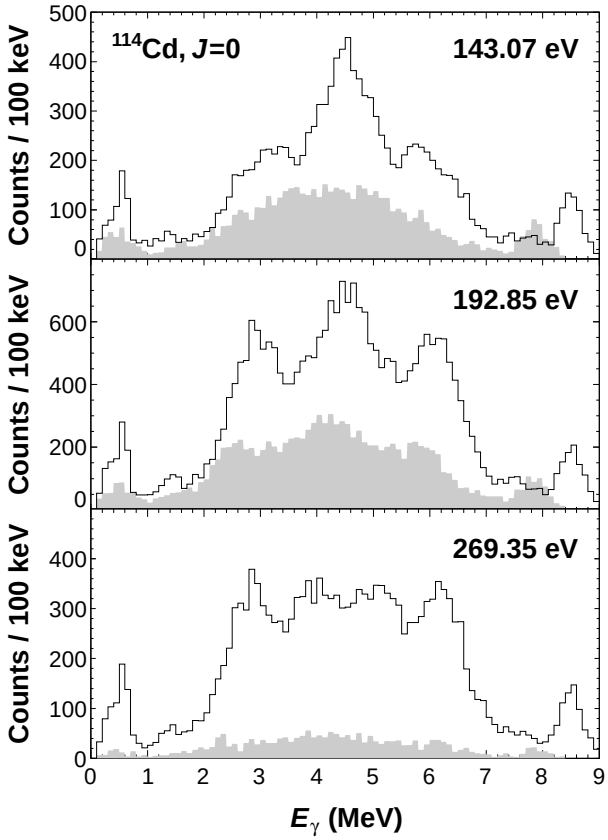

FIG. 5: Two-step cascade spectra from the $J = 0$ capture levels in ^{114}Cd. The resonance energy is given in the top-right corner of each plot. The filled gray histograms correspond to multiplicity 2 spectra in coincidence with the transition from the 2_1^+ level to the ground state at 560 keV. All spectra were collected under the requirement the sum energy of all γ rays registered by DANCE to be within the interval from 8.8 to 9.2 MeV representing the Q value of the ^{113}Cd$(n,\gamma)^{114}$Cd reaction of 9.043 MeV.

cut in the TOF spectrum with a width close to the full width at the half maximum of the resonance (cf. Fig. 2). Spectra of 2 to 8 fold coincidences were sorted out giving the γ-ray intensity for each M_γ cascades.

Two-step cascade (TSC) spectra of γ rays corresponding to two transitions in a cascade starting from the capture level and ending at the ground state or at a low-lying level are of particular interest because of their high sensitivity to the shape of the photon strength function. The TSC spectra from all $J = 0$ and the first five $J = 1$ resonances listed in Table I are shown in Figs. 3, 4, 5, and 6. A noticeable difference between the spectra from $J = 0$ resonances in ^{112}Cd and ^{114}Cd, specifically the highly fed 2_1^+ level in ^{112}Cd, and the similarity between the $J = 0$ and 1 spectra from resonances in ^{112}Cd lead to a doubt in the $J = 0$ assignment of the resonances in ^{112}Cd at 138.11 and 478.01 eV. Spectral shapes thus strongly indicate that both resonances have $J = 1$. Additional arguments for this spin assignment are provided by a comparison with statistical-model simulations presented in Sec. III B.

Noticeable fluctuations in spectral shapes of the TSC spectra are enhanced by the relatively low level density in the cadmium isotopes in comparison with similar experiments in the rare-earth nuclei [27, 28]. The large spacing among the lowest levels in cadmium isotopes provides a clear separation of the peaks in the TSC spectra corresponding to the feeding transitions from the capture to the first and second excited levels and the subsequent transitions from these levels to the ground state. The transitions from the first two excited states are also present in the spectra with M_γ larger than 2. This fea-

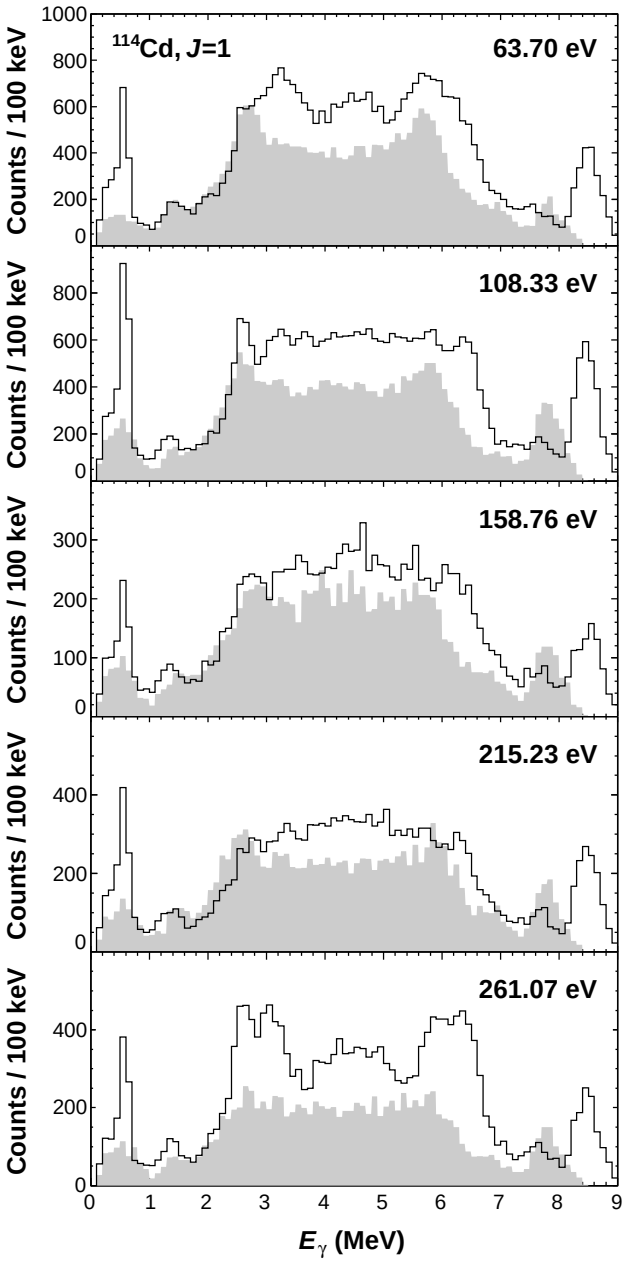

FIG. 6: Analogous to Fig. 5 but for the first five $J = 1$ capture resonances in ^{114}Cd in Table I.

ture allows us to collect spectra in coincidence with the transition from the first excited level to the ground state ($2_1^+ \rightarrow$ g.s.), i.e. requiring one order higher coincidence multiplicity and one of the transitions to be within the energy gate from 0.52 to 0.72 MeV and from 0.45 to 0.65 MeV for the cascades following neutron capture in ^{111}Cd and ^{113}Cd, respectively. Those spectra we will call "gated spectra". The E_γ^{total} and neutron-energy cuts remain the same as for the cascades ending at the ground state. The TSC spectra in coincidence with the transition from the first excited level to the ground state are shown as filled gray histograms in Figs. 3, 4, 5, and 6. Note, the $2_1^+ \rightarrow$ g.s. transition has a similar energy as the $0_2^+ \rightarrow 2_1^+$ transition because the levels are members of a vibrational band. Therefore, even gated on the 620 or 560 keV transitions in ^{112}Cd or ^{114}Cd, respectively, a peak at the same energies still remains.

Due to the significant fluctuations of the TSC spectral shapes from different resonances, comparison with statistical-model calculations can be achieved by averaging the measured spectra. There are two ways to average the spectra (i) by calculating the weighted mean, where the weighting factor depends on the statistics of each spectrum giving a highest weight to the spectra from the strongest resonances and (ii) by averaging without weighting considering only the shape of the spectra and calculating a deviation from the mean value. Both methods provide almost identical mean spectra but with different uncertainties. In this work, we use the second method because we are also interested in the fluctuations of the spectra provided by the variance $\epsilon^2(E_i)$ in addition to the mean values $\bar{A}(E_i)$ calculated for each energy bin E_i of the spectra according to the formulae:

$$\bar{A}(E_i) = \frac{1}{N}\sum_{j=1}^{N} A_j(E_i),$$

$$\epsilon^2(E_i) = \frac{1}{N}\sum_{j=1}^{N}(A_j(E_i) - \bar{A}(E_i))^2, \qquad (1)$$

where N is the number of the spectra to be averaged and $A_j(E_i)$ are the counts in spectrum j at energy bin E_i. Since each resonance has a different (n,γ) cross section and respectively provide different intensity of the cascade transitions, before averaging each spectrum was normalized to unity area.

In addition to the shape of spectra for different multiplicities, we also compare the simulations with the observed multiplicity distribution. The multiplicity distribution of the cascade transitions from each resonance has been obtained from the number of detected γ rays corresponding to each multiplicity with the same restriction on the sum energy as for the TSC spectra. Analogous to the γ-ray spectra, we normalize each multiplicity distribution to unity area to compensate for the differences in the yield due to the different (n,γ) cross sections of the individual resonances. The average value and variance of the multiplicity distribution was calculated according to Eq. (1).

III. SIMULATIONS OF THE γ-RAY CASCADES

A noticeable similarity of the shapes of the TSC spectra from the $J = 1$ resonances in the ^{111}Cd(n,γ) and ^{113}Cd(n,γ) reactions (cf. Figs. 4 and 6) indicates that the PSF governing the γ-ray decay in both cadmium isotopes is very similar. We used the Monte Carlo code `DICEBOX` [29] to simulate the cascade transitions in ^{112}Cd and ^{114}Cd within the statistical model in which a γ-ray

cascade is completely determined by level density, PSF for different types of transitions and fluctuation properties of partial radiation widths. A realization of the real nucleus is created by DICEBOX by building a level scheme and assigning partial widths for transitions from each level to all lower-lying ones. In the cascade simulations for ^{112}Cd and ^{114}Cd, we used the back-shifted Fermi gas model for calculating the level density with level-density parameters of 14.25 and 14.73 MeV^{-1}, respectively, and back-shift energies of 0.77 and 0.92 MeV, respectively, taken from Ref. [30]. The ratio of densities of states with positive and negative parities for a given angular momentum was considered to be equal above excitation energy of 2.5 MeV reflecting the experimental findings from inelastic electron scattering experiments [31, 32]. The Wigner distribution [33] was used for calculating the level spacing fluctuations. The transition widths were assigned from the considered PSFs for $E1$, $M1$ and $E2$ radiation, discussed below, with fluctuations given by the Porter-Thomas distribution [34]. The fluctuations of the transition widths cause differences of the spectral shapes from different realizations analogous to the measured spectra from individual resonances.

Once a nuclear realization is created, DICEBOX simulates the cascade transitions starting from the neutron-capture level and ending at the ground state. The simulation process of DICEBOX is discussed in more detail in Ref. [29]. The simulations in the present work were performed for 100 nuclear realizations and for 10^6 cascades per realization.

A. Photon strength function

The PSFs characterize the probability for γ-ray excitation and de-excitation in the nucleus. They represent the energy distribution of the averaged reduced widths for γ-ray transitions with energy E_γ of type X and multipolarity L [1]. In general, we distinguish two types of PSFs, "upward" $\vec{f}_{XL}(E_\gamma)$ and "downward" $\overleftarrow{f}_{XL}(E_\gamma)$ strength functions. The "upward" PSF is related to the average probability $\langle\Gamma_0^{XL}\rangle$ for γ-ray excitation of a level from the ground state:

$$\vec{f}_{XL}(E_\gamma) = E_\gamma^{-(2L+1)}\frac{\langle\Gamma_0^{XL}(E_\gamma)\rangle}{D(E_x)}, \qquad (2)$$

where $D(E_x)$ is the average spacing of levels at excitation energy E_x. In photoexcitation, E_γ is equal to E_x omitting the negligible recoil energy. In particular for dipole radiation $X1$, Eq. (2) transforms to:

$$\vec{f}_{X1}(E_\gamma) = \frac{2J_0+1}{2J_x+1}\frac{\langle\sigma_\gamma(E_\gamma)\rangle}{(\pi\hbar c)^2 E_\gamma}, \qquad (3)$$

where J_0 and J_x are the angular momenta of the ground state and the excited level, respectively, and $\langle\sigma_\gamma(E_\gamma)\rangle$ is the $E1$ or $M1$ photoabsorption cross section measured in photon-induced experiments (e.g. Refs. [6, 13, 35–37]).

The probability for de-excitation transitions from levels at excitation energy E_x is governed by the "downward" PSF:

$$\overleftarrow{f}_{XL}(E_\gamma) = E_\gamma^{-(2L+1)}\frac{\langle\Gamma_i^{XL}(E_\gamma)\rangle}{D(E_x)}, \qquad (4)$$

where $\Gamma_i^{XL}(E_\gamma)$ is the partial width of a level at E_x for a transition with energy E_γ. Note, $E_\gamma \le E_x$.

While $\vec{f}_{E1}(E_\gamma)$ depends on the photoabsorption cross section, which can be obtained from (γ,γ') and (γ,n) experiments, the "downward" PSF cannot be measured directly because we cannot know from the experiment the initial and final level energy for each transition E_γ. Since the output γ-ray intensity distribution in the (n,γ) reaction depends on the level density and the PSF, the approach we follow in this work to deduce $\overleftarrow{f}_{E1}(E_\gamma)$ is to reproduce the measured γ-ray distribution from the (n,γ) reaction with cascade simulations by fixing the level density and varying the shape of the $E1$ PSF. We also fix the PSFs for $M1$ and $E2$ transitions to the spin-flip $M1$ and the isoscalar $E2$ resonances, respectively, because of their minor contributions to the γ-ray intensity. Lorentzian curves with parameters taken from the systematics in Ref. [38] were used for $\overleftarrow{f}_{M1}(E_\gamma)$ and $\overleftarrow{f}_{E2}(E_\gamma)$, these parameters are summarized in Table II. The exact form of the Brink hypothesis was assumed for $M1$ and $E2$ strength. In addition to the $M1$ spin-flip resonance in $\overleftarrow{f}_{M1}(E_\gamma)$, we added in some of the simulations the low-lying scissors mode in ^{112}Cd and ^{114}Cd investigated in photon-scattering experiments [39].

In this work, we focus on the two $\overleftarrow{f}_{E1}(E_\gamma)$ theoretical models, the standard Lorentzian curve (SLO) and the model of Kadmenskii, Markushev and Furman (KMF). The SLO model [12], known also as Brink-Axel model, is based on exact validity of the Brink hypothesis and Lorentzian extrapolation of $\langle\sigma_\gamma(E_\gamma)\rangle$ at energies below the neutron-separation energy. It has been demonstrated for deformed nuclei [3, 4] that the GDR tail is well reproduced by a superposition of three Lorentzian curves with equal widths Γ_G and integrals, but maxima E_i inversely reciprocal to the semi-axes of the deformed ellipsoid, i.e. for even-even nuclei:

$$\overleftarrow{f}_{E1}(E_\gamma) = \frac{1}{3(\pi\hbar c)^2}\sum_{i=0}^{2}\frac{\sigma_0 E_\gamma \Gamma_G^2}{(E_\gamma^2 - E_i^2)^2 + E_\gamma^2\Gamma_G^2}, \qquad (5)$$

where σ_0 and Γ_G are the cross section at the maximum of the Lorentz curve and its width. The energies of the maxima E_i $(i = 0, 1, 2)$ can be calculated using the Hill-Wheeler parameters β_2 and γ according to the relation [41]:

$$E_i = E_G \exp\left(-\sqrt{\frac{5}{4\pi}}\beta_2\cos(\gamma - \frac{2}{3}\pi i)\right), \qquad (6)$$

where E_G is the energy of the GDR maximum if the nucleus were spherical.

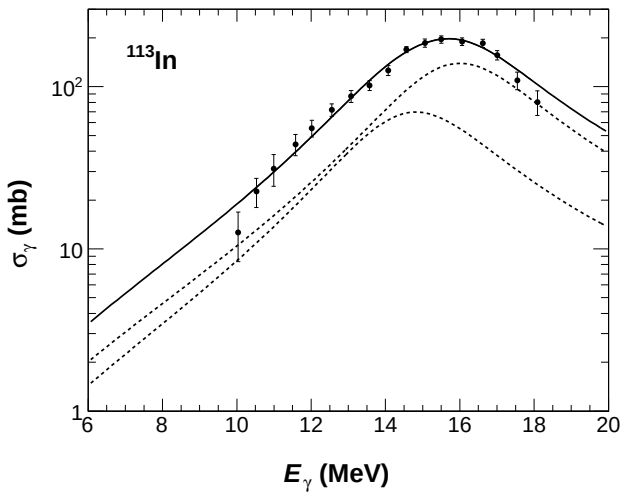

FIG. 7: Fit of the ^{113}In(γ,n) cross section [40] (data points) with a Lorentzian (solid curve) represented as a composition of two Lorentzians (dashed curves) according to Eq. (5). The deformation parameter γ was found to be 0° from the fit (i.e. axial symmetry) therefore two Lorentzians sum up to the one shown with higher-energy maximum. The parameters obtained from the fit were used to estimate the GDRs in ^{112}Cd and ^{114}Cd.

We obtained the GDR parameters from experimental data. The ^{112}Cd(γ,n) and ^{114}Cd(γ,n) reactions have not been measured, therefore we used the data from ^{113}In(γ,n) [40] to estimate the GDR parameters E_G, σ_0 and Γ_G for the considered cadmium isotopes. This approach is reasonable because it is known from systematics that the GDR parameters vary slowly in neighboring nuclei. A fit of the ^{113}In(γ,n) cross section with a function according to Eqs. (3) and (5) is shown in Fig. 7. The deformation parameters were kept free in the fit and the obtained values of $\gamma = 0°$ and $\beta_2 = 0.082$, describing ^{113}In as an axially symmetric nucleus, are in fair agreement with the theoretical predictions from Ref. [42]. The GDR cross section in ^{112}Cd and ^{114}Cd was calculated from Eq. (5) using the parameters $E_G = 15.6$ MeV, $\sigma_0 = 69.7$ mb and $\Gamma_G = 4.4$ MeV from the fit of the ^{113}In(γ,n). The σ_0 was scaled to the cadmium isotopes using the Thomas-Reiche-Kuhn sum rule [43] and the energies E_i were calculated from Eq. (6) for deformation parameters taken from potential-energy surface mapping calculations [44] of $\beta_2 = 0.133$ and 0.150, respectively. The GDR parameters used in the statistical simulations are summarized in Table II.

The KMF model [45] has been derived from the theory of Fermi liquids [46] for the limit of $E_\gamma \ll E_G$:

$$\overleftarrow{f}_{E1}(E_\gamma,T) = \frac{0.7}{3(\pi\hbar c)^2}\frac{\sigma_0 E_G \Gamma_G \Gamma(E_\gamma,T)}{(E_\gamma^2 - E_G^2)^2}, \qquad (7)$$

where

$$\Gamma(E_\gamma,T) = \Gamma_G \frac{E_\gamma^2 + 4\pi^2 T^2}{E_G^2},$$

Structure	E_G (MeV)	σ_0 (mb)	Γ_G (MeV)
^{112}Cd			
Giant dipole resonance ($E1$)	15.56	69.2	4.3
Pygmy dipole resonance ($E1$)	6.3	10.5	2
Spin-flip resonance ($M1$)	8.51	0.789	4.0
Scissors mode resonance ($M1$)	3.33	0.0364	1.0
Quadrupole resonance ($E2$)	13.0	2.54	4.75
^{114}Cd			
Giant dipole resonance ($E1$)	15.56	70.1	4.3
Pygmy dipole resonance ($E1$)	6.3	10.5	2
Spin-flip resonance ($M1$)	8.46	0.774	4.0
Scissors mode resonance ($M1$)	3.33	0.0364	1.0
Quadrupole resonance ($E2$)	13.0	2.54	4.75

TABLE II: Parameters of the Lorentzian curves used to calculate the strength functions for $E1$, $M1$ and $E2$ transitions in the cascade simulations for ^{112}Cd and ^{114}Cd.

and $T = \sqrt{(E_x - E_\gamma - \Delta)/a}$ is the temperature of the nucleus at a level with energy E_x, Δ and a are the pairing energy and the level density parameter, respectively. The parameters E_G, σ_0 and Γ_G, used in this model, are the same ones used in the SLO model.

We also considered in some of the simulations a pygmy dipole resonance superimposed on the GDR tail. The PDR was represented by a Lorentzian curve with a width of 2 MeV and a height adjusted such that the PDR integral is 2% of the Thomas-Reiche-Kuhn sum rule: $\frac{\pi}{2}\sigma_0\Gamma_G = 0.02 \times 60NZ/A$, which is a typical value obtained for the $N = 50$ isotones [5]. The PDR position was chosen such that it reproduces the "shoulder" around 6 MeV in the M_γ=3 spectra (cf. Fig. 8). The PDR parameters used in the statistical simulations are given in Table II.

B. Comparison with measured spectra

The γ-ray cascades simulated with `DICEBOX` were used as input to `Geant4` [47] simulations of the DANCE detector response [48]. The simulations were verified with the measurements with the ^{22}Na and ^{88}Y sources. The deposited energy in each BaF_2 crystal was smeared with a Gaussian function with a width adjusted to reproduce the peaks from the source measurements. An add-back procedure was applied, analogously to the measurement, when neighboring crystals fired and spectra of two-, three- and multi-fold coincidences collected. We also prepared simulated spectra gated on the transition from the first 2^+ level to the ground state applying the same energy windows as the ones for the measured spectra. The detector-response simulations were performed for each `DICEBOX` nuclear realization separately and mean spectra and variances were calculated according to Eq. (1). We used χ^2 to estimate the agreement between the measured and simulated mean spectra consisting of N

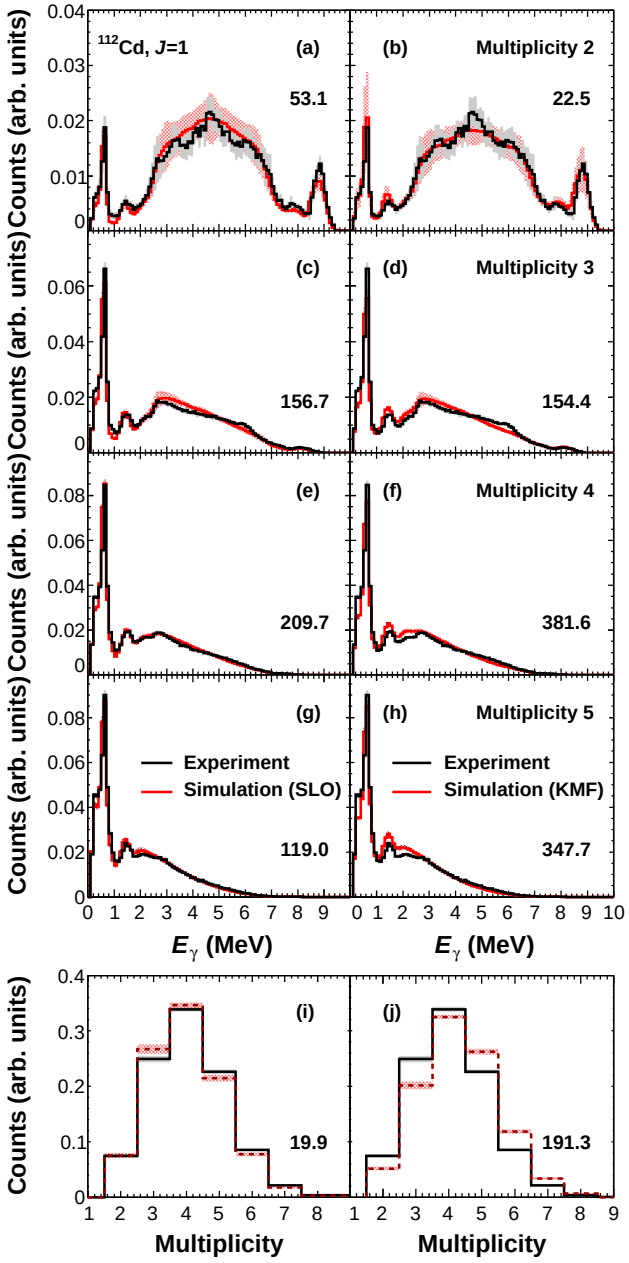

FIG. 8: (Color online) Comparison of the mean measured spectra from $J = 1$ resonances in ^{112}Cd for multiplicities 2 (a) and (b), 3 (c) and (d), 4 (e) and (f) and 5 (g) and (h) in black with cascade simulations in dashed red histograms using the SLO model for the $E1$ PSF (left panels (a), (c), (e), (g) and (i)) and the KMF model (right panels (b), (d), (f), (h) and (j)). The shaded gray and light red areas represent one standard deviation from the mean value in the measured and simulated spectra, respectively. The multiplicity distributions are shown in the bottom figures. All histograms were normalized to unity area. Calculated χ^2 values are given in each panel.

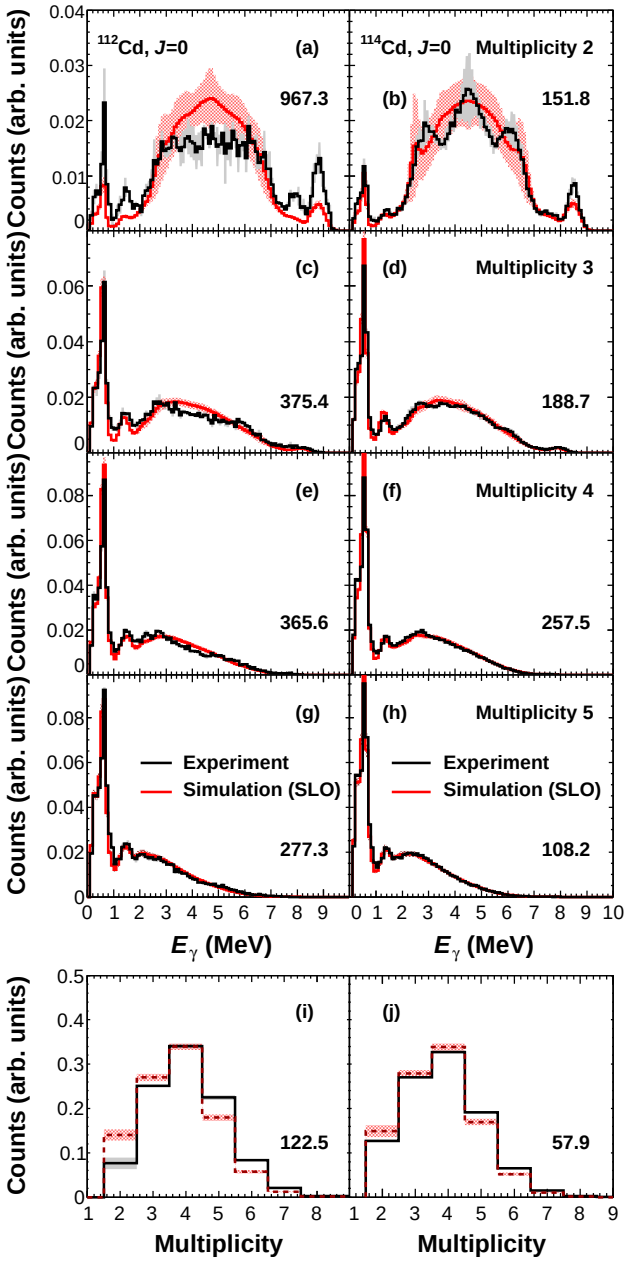

FIG. 9: (Color online) Comparison of measured and simulated spectra using the SLO model for the cascade transitions from the $J = 0$ resonances in ^{112}Cd (left panels (a), (c), (e), (g) and (i)) and ^{114}Cd (right panels (b), (d), (f), (h) and (j)). See Fig. 8 for the notations.

number of bins according to the relation:

$$\chi^2 = \sum_{i=1}^{N} \frac{\left(\bar{A}_{exp}(E_i) - \bar{A}_{sim}(E_i)\right)^2}{\epsilon^2_{exp}(E_i) + \epsilon^2_{sim}(E_i)}, \qquad (8)$$

where $\bar{A}_{exp}(E_i)$ and $\bar{A}_{sim}(E_i)$ are the counts in an energy bin at E_i in the measured and simulated mean spectrum, respectively, and $\epsilon^2_{exp}(E_i)$ and $\epsilon^2_{sim}(E_i)$ are the corresponding variances. The typical degree-of-freedom for

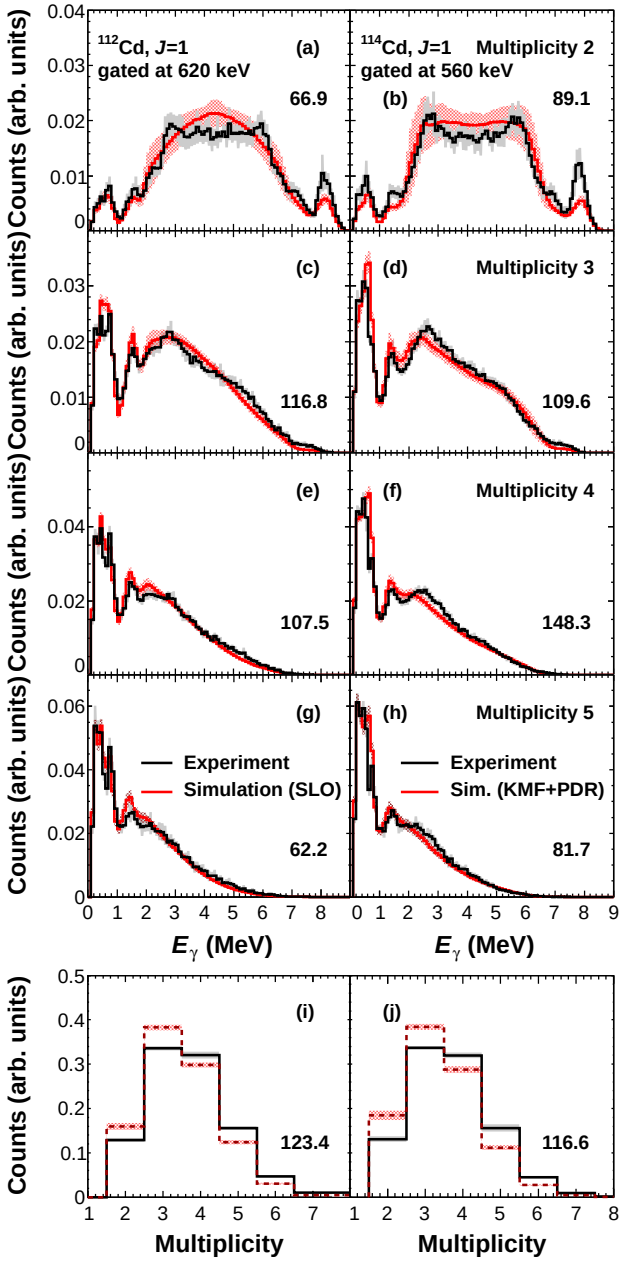

FIG. 10: (Color online) Comparison of measured and simulated spectra using the SLO model for the cascade transitions from the $J = 1$ resonances in ^{112}Cd (left panels (a), (c), (e), (g) and (i)) and ^{114}Cd using the KMF model with PDR (right panels (b), (d), (f), (h) and (j)) in coincidence with the transitions from the first excited level to the ground state. See Fig. 8 for the notations.

our spectra with binning of 100 keV/channel is from 45 for M_γ=8 to 90 for M_γ=2.

An additional quantity from the simulations, which can be compared with the experimental data, is the total radiative width, Γ_γ, of s-wave neutron resonances. This is an integral quantity equal to the sum of all partial widths for γ-ray transitions from the capture state to the lower-lying levels. The total radiative width for each nuclear realization is calculated by DICEBOX from the assigned partial decay widths from the PSF and level density models. The Γ_γ's averaged over 100 realizations and their variances are given in Table III. These values can be compared with the averaged values for $J = 0$ and 1 resonances from Table I of 96(12) and 105(10) meV for ^{112}Cd and 105(5) and 101(9) meV for ^{114}Cd, respectively.

Comparisons of the measured MSC spectra from the $J = 1$ resonances in ^{112}Cd with simulations using the SLO and KMF models are shown in Fig. 8. The two PSF models give a good representation of the shape of the γ-ray spectra, but the simulations with the KMF model fail to reproduce the measured multiplicity distribution. Similar results were obtained for the spectra from the $J = 1$ resonances in ^{114}Cd (not shown). The comparison with the measured spectra is practically the same if the scissors mode resonance is excluded from the $M1$ PSF in the DICEBOX simulations and worsen when a PDR is added to the SLO PSF. On the other hand the PDR improves the simulations when included with the KMF PSF. The χ^2 values are listed in Table III for all considered PSF models.

Despite the small number of known $J = 0$ resonances in both isotopes, we observe a good agreement of the simulations using the SLO model with the γ-ray spectra from ^{114}Cd, shown in Fig. 9. The TSC spectra from the $J = 0$ resonances in ^{112}Cd (cf. Fig. 9), as was mentioned above, display a shape contradictory to that expected and seen from the $J = 0$ resonances in ^{114}Cd. Because the angular momentum of the capture level is $J^\pi = 0^+$, only an $E2$ transition is possible to the first excited 2^+ state, which is much less probable than the $E1$ and $M1$ transitions contributing to the middle part of the spectrum, i.e. we would expect the peak at 620 keV to be smaller than the intensity at the middle part of the spectrum, as seen for the two-step cascade spectra from the $J = 0$ resonances in ^{114}Cd in Fig. 9. In addition, the multiplicity 2 spectra from the $J = 0$ resonances in ^{112}Cd have very similar shape to the ones from the $J = 1$ resonances (cf. Fig. 8). Also, the predicted shape of the multiplicity 3 spectrum strongly deviates from the measured one from ^{112}Cd, while it reasonably fits data from ^{114}Cd. These arguments strongly speak in favor of a misassignment of the resonance spin in Ref. [22]. Our analysis of the spectra indicates that both resonances should have spin $J = 1$. This change would allow a reasonable description of the spectra with the models used in our simulations.

Gated MSC spectra from the $J = 1$ resonances in ^{112}Cd and ^{114}Cd are shown in Fig. 10. The TSC spectra seem to change the shape of the middle part of the spectrum from convex in the cascades terminated at the ground state (cf. Fig. 8) to concave in the spectra gated on the $2_1^+ \rightarrow g.s.$ transitions (cf. Fig. 10). This behavior could be a signature for change of the $E1$ PSF shape between 3 and 6 MeV. The comparison in Fig. 10 shows that the SLO model, which described well the cascades terminated at the ground state (cf. Fig. 8), provides a

PSF model				γ-ray spectra of multiplicity							Multiplicity	Γ_γ[e]
SLO[a]	KMF[b]	PDR[c]	SM[d]	2	3	4	5	6	7	8	distribution	(meV)
Cascades from $J=0$ resonances in ^{111}Cd(n,γ) terminated at the ground state												
✓	-	-	-	966.0	360.8	337.1	260.6	113.6	65.9	39.2	107.5	188(10)
✓	-	-	✓	967.3	375.4	365.6	277.3	119.4	66.3	39.5	122.5	190(10)
-	✓	-	✓	352.5	226.2	444.2	573.4	279.7	133.4	50.4	68.8	131(4)
✓	✓	-	✓	832.6	149.5	143.9	155.0	115.8	87.2	42.3	19.7	154(8)
Cascades from $J=0$ resonances in ^{111}Cd(n,γ) gated on 620 keV												
✓	-	-	-	268.3	302.1	315.5	152.7	49.7	47.1	14.4	363.4	188(10)
✓	-	-	✓	277.3	310.3	347.3	159.2	49.1	45.9	12.7	430.2	190(10)
-	✓	-	✓	122.3	303.0	437.1	328.1	95.2	59.4	34.3	8.4	131(4)
✓	✓	-	✓	139.3	137.8	180.0	134.8	80.6	52.9	27.5	48.3	154(8)
Cascades from $J=1$ resonances in ^{111}Cd(n,γ) terminated at the ground state												
✓	-	-	-	52.4	142.2	187.0	119.1	54.9	17.1	7.3	12.1	188(7)
✓	-	-	✓	53.1	156.7	209.7	119.0	55.8	17.2	7.2	19.9	191(7)
✓	-	✓	✓	175.2	144.3	224.0	143.5	55.7	19.6	7.3	146.5	366(19)
-	✓	-	✓	22.5	154.4	381.6	347.7	137.2	39.9	10.4	191.3	131(2)
-	✓	✓	✓	162.0	110.5	213.7	142.1	63.3	21.3	7.1	46.9	306(15)
✓	✓	-	✓	27.9	76.4	227.5	186.4	81.5	29.0	9.5	23.5	155(5)
Cascades from $J=1$ resonances in ^{111}Cd(n,γ) gated on 620 keV												
✓	-	-	-	67.7	107.7	102.5	62.7	19.3	6.3	4.6	102.2	188(7)
✓	-	-	✓	66.9	116.8	107.5	62.2	19.1	6.1	4.5	123.4	191(7)
✓	-	✓	✓	126.7	143.4	148.9	57.8	20.4	6.8	3.8	309.4	366(19)
-	✓	-	✓	37.3	175.9	215.5	122.7	32.0	8.0	6.9	50.5	131(2)
-	✓	✓	✓	85.6	132.0	139.7	64.9	22.4	6.0	4.3	170.1	306(15)
✓	✓	-	✓	42.3	149.0	153.5	86.5	27.0	7.6	6.0	1.8	155(5)
Cascades from $J=0$ resonances in ^{113}Cd(n,γ) terminated at the ground state												
✓	-	-	-	149.7	181.6	245.4	113.8	46.9	26.9	13.3	49.2	154(10)
✓	-	-	✓	151.8	188.7	257.5	108.2	47.4	28.3	13.0	57.9	156(10)
-	✓	-	✓	65.8	229.1	587.5	483.9	195.2	71.5	27.9	165.1	109(4)
✓	✓	-	✓	85.4	142.3	300.3	168.3	84.2	40.9	22.8	16.1	126(8)
Cascades from $J=0$ resonances in ^{113}Cd(n,γ) gated on 560 keV												
✓	-	-	-	79.6	241.2	147.2	66.3	38.4	18.3	6.4	195.5	154(10)
✓	-	-	✓	80.1	226.7	145.7	67.0	38.2	18.4	5.4	221.3	156(10)
-	✓	-	✓	44.5	217.1	351.7	150.5	69.9	34.7	13.9	65.4	109(4)
✓	✓	-	✓	80.6	233.8	213.4	105.3	54.7	30.1	10.6	2.9	126(8)
Cascades from $J=1$ resonances in ^{113}Cd(n,γ) terminated at the ground state												
✓	-	-	-	50.2	154.7	156.3	103.4	49.3	14.6	7.3	7.5	152(6)
✓	-	-	✓	50.0	162.9	172.9	102.7	46.2	16.2	8.2	12.3	154(6)
✓	-	✓	✓	134.5	128.1	171.3	113.8	47.3	13.3	7.2	73.0	282(17)
-	✓	-	✓	35.9	183.8	400.1	393.2	161.5	36.0	11.2	154.0	109(2)
-	✓	✓	✓	107.1	88.2	163.7	106.1	44.5	12.4	7.1	20.6	237(12)
✓	✓	-	✓	21.2	88.0	218.1	185.3	81.8	23.9	9.7	28.0	125(4)
Cascades from $J=1$ resonances in ^{113}Cd(n,γ) gated on 560 keV												
✓	-	-	-	104.3	130.8	108.7	61.5	17.2	6.5	4.3	64.8	152(6)
✓	-	-	✓	105.0	132.9	111.2	63.1	18.0	7.1	4.0	76.2	154(6)
✓	-	✓	✓	139.4	122.5	132.2	78.5	21.5	8.4	3.6	223.8	282(17)
-	✓	-	✓	47.5	162.6	266.1	128.1	29.3	11.0	7.2	47.1	109(2)
-	✓	✓	✓	89.1	109.6	148.3	81.7	22.1	9.6	4.3	116.6	237(12)
✓	✓	-	✓	20.3	116.4	147.1	86.4	24.5	9.5	6.0	0.4	125(4)

[a]Standard Lorentzian model.
[b]Model of Kadmenskii, Markushev and Furman.
[c]Pygmy dipole resonance.
[d]Scissors mode resonance.
[e]Total radiative width.

TABLE III: Calculated χ^2 values from the comparison of the measured γ-ray spectra for multiplicities from 2 to 8 and the multiplicity distributions with the simulations for various PSF models. The symbol "✓" depicts the considered PSF model in the simulations. If the SLO-KMF model was used then "✓" in the columns corresponding to both the SLO and KMF models. The degree-of-freedom of the MSC spectra is from 45 for multiplicity 8 to 90 for multiplicity 2 spectra and 6 for the multiplicity distributions.

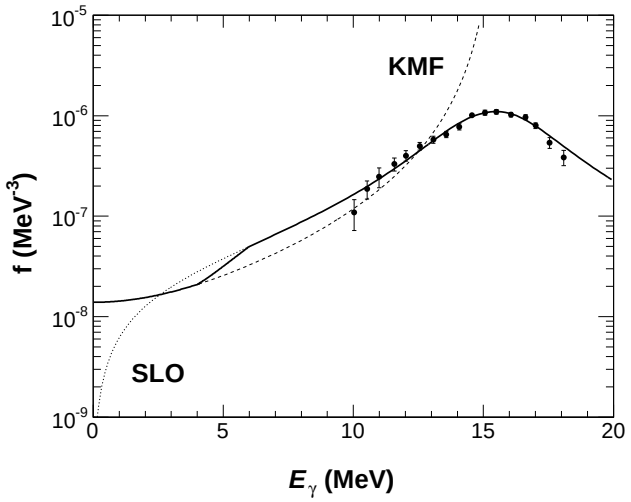

FIG. 11: An $E1$ PSF (solid curve) model consisting of KMF (dashed curve) for $E_\gamma < 4$ MeV and SLO (dotted curve) for $E_\gamma > 6$. A linear combination of both models is used for E_γ between 4 and 6 MeV. The data points represent the strength function calculated from the ^{113}In(γ, n) cross section and used to obtain the GDR parameters for ^{112}Cd and ^{114}Cd.

poor agreement with the two-step cascade spectra and the multiplicity distributions for the cascades in coincidence with the $2_1^+ \rightarrow g.s.$ transitions in both isotopes. The simulations with the KMF model also fail to reproduce the gated TSC spectra and the multiplicity distributions. Including a PDR superimposed on the $E1$ PSF leads to a slight visual improvement of the shape of the middle part of the simulated TSC spectrum but it still cannot fully reproduce the concave shape. At the same time, the overall χ^2 increases. It means that postulation of the PDR in the $E1$ PSF does not lead to a better agreement between experiment and simulations. An example of an $E1$ PSF consisting of SLO model and PDR is given for ^{114}Cd in Fig. 10.

C. Combined SLO and KMF model

The interesting change in the shape of the spectra of TSCs terminated at the ground state in comparison with those terminated at the first excited levels (the gated TSC spectra) cannot be reproduced by a smooth PSF, but as mentioned above requires a PSF with a rather strong change of the slope at E_γ between 3 and 6 MeV. A strong enhancement of the $E1$ PSF at 6 MeV with respect to 4 or 5 MeV will increase the γ-ray intensity at 6 and 3 MeV relative to the middle part of the spectrum (cf. Fig. 10). The same expectation is valid if the PSF is larger at 3 MeV than at 4 or 5 MeV. The scissors mode resonance and PDR are located in this energy range and may, in general, affect the simulated spectra. However, as we discussed above, we could not reproduce correctly the shapes of the gated spectra and multiplicity distributions

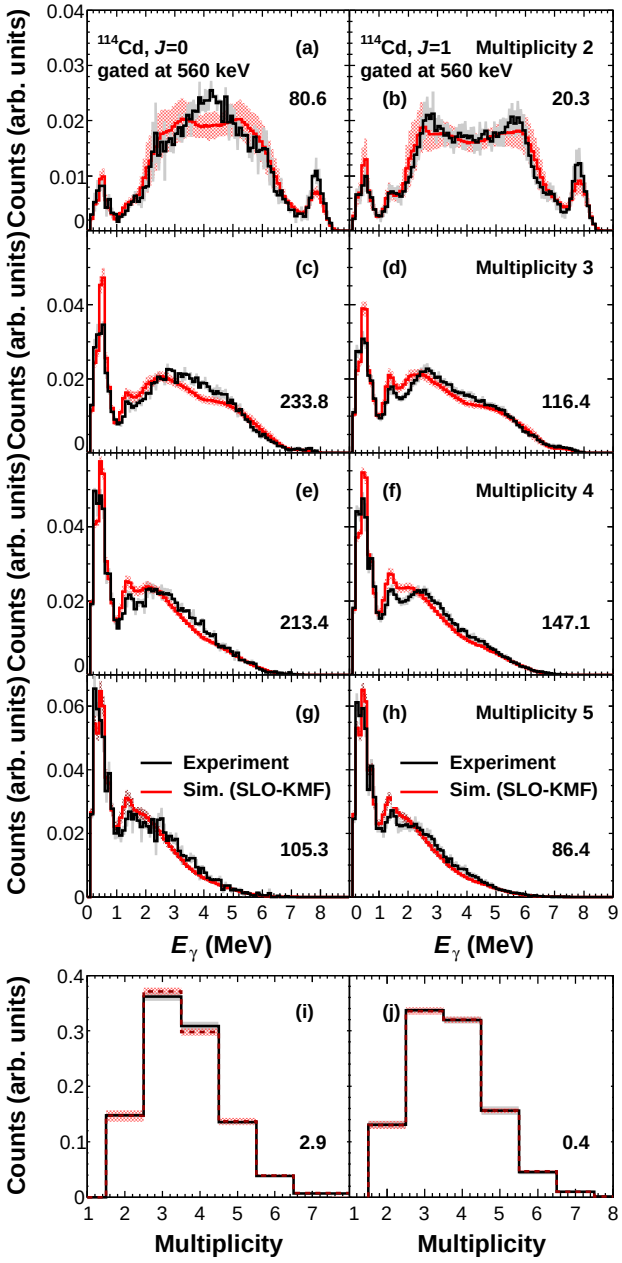

FIG. 12: (Color online) Comparison of the measured cascade transitions from the $J = 0$ (left panels (a), (c), (e), (g) and (i)) and $J = 1$ (right panels (b), (d), (f), (h) and (j)) resonances in ^{114}Cd in coincidence with the transition from the first excited level to the ground state and corresponding simulations using the combined SLO and KMF model. See Fig. 8 for the notations.

when we added the scissors mode resonance and/or PDR to the $M1$ and $E1$ PSFs, respectively, cf. Table III and Fig. 10.

A suggestion to match the SLO model with the KMF model made for the rare-earth nuclei [49] would provide the necessary rapid change of PSF. Such a model uses the advantages of both theoretical models. The standard Lorentzian is a good PSF model for γ rays with energies

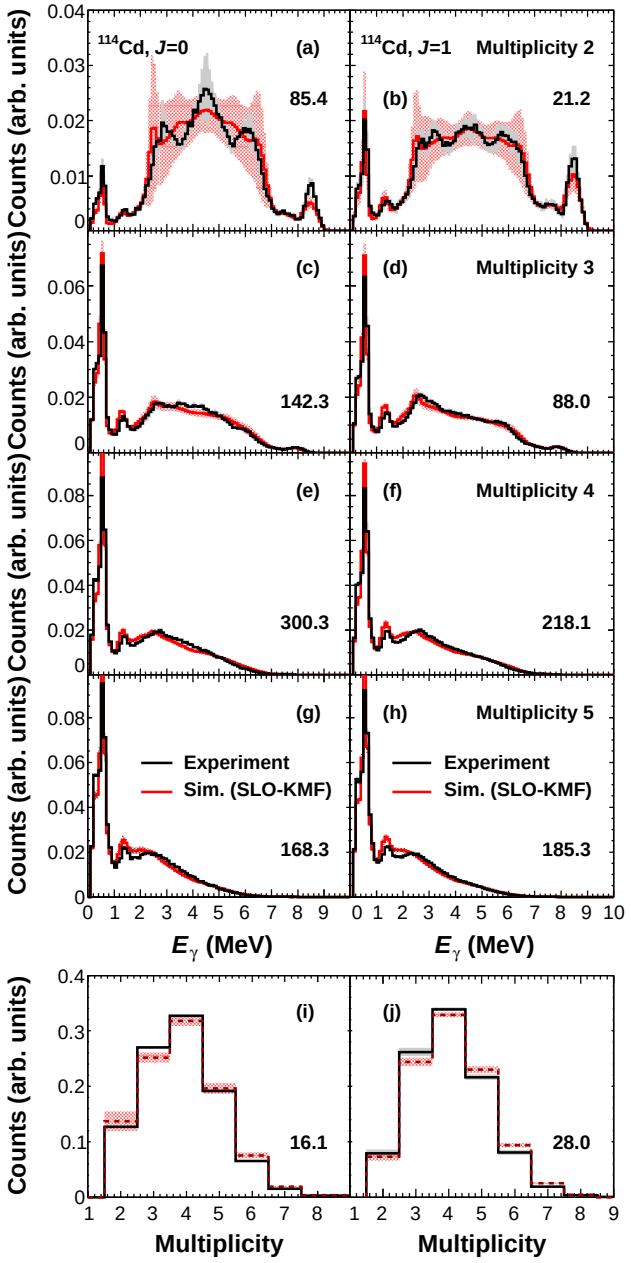

FIG. 13: (Color online) Comparison of the measured and simulated spectra for the cascade transitions from the $J = 0$ (left panels (a), (c), (e), (g) and (i)) and $J = 1$ (right panels (b), (d), (f), (h) and (j)) resonances in ^{114}Cd. The combined SLO and KMF model was used in the simulations. See Fig. 8 for the notations.

close to the neutron-separation energy because of its excellent description of GDR. In contrast to SLO, the KMF model has been derived to be a good approximation of the photon strength at γ-ray energies much smaller than the GDR maximum, i.e. $E_\gamma \to 0$ MeV. We constructed an $E1$ PSF from the SLO and KMF models in the following way: below $E_\gamma = 4$ MeV and above $E_\gamma = 6$ MeV we considered the pure KMF and SLO models, respectively, and we used a linear combination of the two models for E_γ between 4 and 6 MeV. The combined SLO and KMF (SLO-KMF) model can be written analytically for E_γ in MeV as:

$$\overleftarrow{f}_{E1}(E_\gamma) = \overleftarrow{f}^{KMF}_{E1}(E_\gamma), \text{ for } E_\gamma \le 4\,\text{MeV},$$
$$\overleftarrow{f}_{E1}(E_\gamma) = \frac{E_\gamma - 4}{2}\,\overleftarrow{f}^{KMF}_{E1}(E_\gamma) + \frac{E_\gamma - 4}{2}\,\overleftarrow{f}^{SLO}_{E1}(E_\gamma), \text{ for } 4\,\text{MeV} < E_\gamma \le 6\,\text{MeV},$$
$$\overleftarrow{f}_{E1}(E_\gamma) = \overleftarrow{f}^{SLO}_{E1}(E_\gamma), \text{ for } E_\gamma > 6\,\text{MeV}. \quad (9)$$

Figure 11 shows a graphical representation of Eq. (9).

A comparison of gated spectra simulated with the SLO-KMF model and measured from capture levels with $J = 0$ and 1 in ^{114}Cd is shown in Fig. 12. The multiplicity distributions are represented correctly by the SLO-KMF model, the two-step cascade spectra have a pronounced concave shape in the middle part, but the γ-ray spectra with multiplicities higher than 2 are not as well reproduced as with the SLO model alone (cf. Fig. 10). We obtained a similar agreement for cascades from the resonances in ^{112}Cd (not shown).

A comparison of the predictions with the SLO-KMF model with the experimental data for spectra terminating at the ground state is given in Fig. 13. As can be seen, the model is able to describe the change in the shapes between the gated and standard TSC spectra from $J = 1$ resonances. Overall the shapes of the higher multiplicity γ-ray spectra are well reproduced, but the multiplicity distributions deviate slightly in comparison with the simulations with the SLO model (cf. e.g. Fig. 8).

The total radiative widths calculated using the SLO-KMF model are about 50% and 25% larger than the measured ones for ^{112}Cd and ^{114}Cd, respectively. Note, that the total radiative width strongly depends on the level density model used in the simulations, if the constant temperature model were selected then the calculated Γ_γ would be at least a factor of two smaller than the one obtained in the current simulations with the back-shifted Fermi gas model, which is much a larger deviation from the measured values.

Although the SLO-KMF model gives an acceptable representation of the cascade transitions in ^{112}Cd and ^{114}Cd, it introduces two additional parameters. The linear combination of the SLO and KMF curves (cf. Eq. (9)) between 4 and 6 MeV provided the desired stiffness of the PSF, but the energy range for matching the two models was selected to reproduce well the cadmium data. A further test of the applicability of the SLO-KMF model over many nuclei is desirable. An indication of its applicability in the medium-mass nuclei are the PSFs deduced from the ^{117}Sn(^{3}He, ^{3}He$'\gamma$) [14] and ^{106}Cd(^{3}He,α)^{105}Cd [15] reactions which clearly can be constructed from the SLO and KMF models with a linear combination of them between 4 and 7 MeV (cf. Fig. 3 in Ref. [14] and Fig. 10 in Ref. [15]), i.e. in a similar range as proposed by our analysis of the ^{112}Cd and ^{114}Cd data.

IV. SUMMARY AND CONCLUSIONS

Cascade γ-ray transitions in ^{112}Cd and ^{114}Cd have been studied in a neutron-capture experiment on natural cadmium using the DANCE calorimeter at LANSCE. Spectra of γ-ray cascades of multiplicities 2 and higher have been collected from known s-wave resonances with $J = 0$ and 1. We observe pronounced fluctuations in the shapes of the TSC spectra from the individual neutron resonances due to the relatively low level density of the cadmium isotopes. The size of the experimentally observed fluctuations seem to be in reasonable agreement with predictions based on the Porter-Thomas fluctuations of individual transition intensities. Cascades of γ rays terminated at the first excited level were studied as well, using a gating on the peak from the $2_1^+ \rightarrow g.s.$ transition. An interesting phenomenon of the measured γ-ray cascades seems to be a change in the shape of the TSC spectra from $J = 1$ resonances terminating at the ground and at the first excited states between E_γ of 3 and 6 MeV. The concave shape for TSC spectra terminating at the ground state becomes convex in the gated TSC spectra.

In the course of analysis of the neutron-capture data we noticed that the spectra of the two $J = 0$ resonances in ^{112}Cd have very similar shape to the ones from the $J = 1$ levels. A possible $J = 0$ misassignment of these levels can explain the large discrepancy with the `DICEBOX` simulations. Further measurements on isotopically enriched ^{112}Cd sample could help to explain this problem.

The shape of the γ-ray spectra of multiplicities from 2 to 8 together with the multiplicity distributions were compared with results from simulations of the cascade transitions with the code `DICEBOX` based on the statistical model. Using these simulations, we obtained information about $E1$ PSF keeping the level density, $M1$ and $E2$ PSFs fixed. The back-shifted Fermi gas model was used for the level density model while the parameters for $M1$ and $E2$ PSFs were taken from systematics. We tested two theoretical $E1$ PSF models, SLO and KMF, and a model which combines them. In addition, we considered the possibility of the presence of the scissors-mode resonance in $M1$ PSF and PDR in $E1$ PSF. The major conclusions from the comparison of the simulations to experimental data can be summarized as:

(i) The KMF model is unable to describe either the shape of the TSC spectra or the observed multiplicity distribution.

(ii) The SLO model gives the best description of the cascades terminated at the ground state, but it is unable to describe gated MSC spectra. In addition, this model fails to reproduce the total radiative width of the neutron resonances.

(iii) Including the scissors-mode resonance and/or PDR to corresponding PSFs provides a minor change of the simulations in comparison with the results from the SLO or KMF models alone.

(iv) The best overall agreement with experimental data is obtained with the SLO-KMF model.

In conclusion, it should be stressed that there are still many unresolved problems related to PSFs in medium-mass nuclei and further study is inevitable. In addition, (γ, n) measurements of the giant dipole resonances in the cadmium isotopes are desirable to constrain the PSF models better.

Acknowledgments

This work benefited from the use of the LANSCE facility and the Manuel J. Lujan, Jr. Neutron Scattering Center. The work has been supported by the NNSA Office of Nonproliferation and Verification Research and Development performed under the US Department of Energy contract DE-AC52-06NA25396. MK acknowledges the support from the Czech Science Foundation under Grand 13-07117S and research plan MSM 0021620859 of the Ministry of Education.

[1] G. A. Bartholomew, E. D. Earle, A. J. Ferguson, J. W. Knowles, and M. A. Lone, Adv. Nucl. Phys. **7**, 229 (1973).
[2] W. Hauser and H. Feshbach, Phys. Rev. **87**, 366 (1952).
[3] A. R. Junghans, G. Rusev, R. Schwengner, A. Wagner, and E. Grosse, Phys. Lett. **B670**, 200 (2008).
[4] G. Rusev, R. Schwengner, F. Dönau, M. Erhard, E. Grosse, A. R. Junghans, K. Kosev, K. D. Schilling, A. Wagner, F. Bečvář, et al., Phys. Rev. C **77**, 064321 (2008).
[5] R. Schwengner, G. Rusev, N. Tsoneva, N. Benouaret, R. Beyer, M. Erhard, E. Grosse, A. R. Junghans, J. Klug, K. Kosev, et al., Phys. Rev. C **78**, 064314 (2008).
[6] A. P. Tonchev, S. L. Hammond, J. H. Kelley, E. Kwan, H. Lenske, G. Rusev, W. Tornow, and N. Tsoneva, Phys. Rev. Lett. **104**, 072501 (2010).
[7] M. Krtička, F. Bečvář, I. Tomandl, G. Rusev, U. Agvaanluvsan, and G. E. Mitchell, Phys. Rev. C **77**, 054319 (2005).
[8] M. Krtička, F. Bečvář, J. Honzátko, I. Tomandl, M. Heil, F. Käppeler, R. Reifarth, F. Voss, and K. Wisshak, Phys. Rev. Lett. **92**, 172501 (2004).
[9] T. S. Tveter, L. Bergholt, M. Guttormsen, E. Melby, and J. Rekstad, Phys. Rev. Lett. **77**, 2404 (1996).
[10] A. Voinov, M. Guttormsen, E. Melby, J. Rekstad, A. Schiller, and S. Siem, Phys. Rev. C **63**, 044313 (2001).
[11] U. Kneissl, H. H. Pitz, and A. Zilges, Prog. Part. Nucl. Phys. **37**, 349 (1996).
[12] P. Axel, Phys. Rev. **126**, 671 (1962).
[13] C. T. Angell, S. L. Hammond, H. J. Karwowski, J. H. Kelley, M. Krtička, E. Kwan, A. Makinaga, and G. Rusev, Phys. Rev. C **86**, 051302(R) (2012).
[14] U. Agvaanluvsan, A. C. Larsen, R. Chankova, M. Guttormsen, G. E. Mitchell, A. Schiller, S. Siem, and A. Voinov, Phys. Rev. Lett. **102**, 162504 (2009).

[15] A. C. Larsen, I. E. Ruud, A. Bürger, S. Goriely, M. Guttormsen, A. Görgen, T. W. Hagen, S. Harissopulos, H. T. Nyhus, T. Renstrøm, et al., Phys. Rev. C **87**, 014319 (2013).

[16] H. Lehmann, A. Nord, A. E. de Almeida Pinto, O. Beck, J. Besserer, P. von Brentano, S. Drissi, T. Eckert, R.-D. Herzberg, D. Jäger, et al., Phys. Rev. C **60**, 024308 (1999).

[17] D. Bandyopadhyay, C. C. Reynolds, C. Fransen, N. Boukharouba, M. T. McEllistrem, and S. W. Yates, Phys. Rev. C **67**, 034319 (2003).

[18] P. W. Lisowski and K. F. Schoenberg, Nucl. Instrum. Methods A **562**, 910 (2006).

[19] M. Mocko, G. Muhrer, F. Tovesson, and J. Ullmann, *Proceedings of the International Topical Meeting on Nuclear Research Applications and Utilization of Accelerators*, Vienna, May 4-8, **AP/IE-03** (2009).

[20] M. Mocko and G. Muhrer, Nucl. Instrum. Methods A **704**, 27 (2013).

[21] M. Jandel, T. A. Bredeweg, E. M. Bond, M. B. Chadwick, R. R. Clement, A. Couture, J. M. O'Donnell, R. C. Haight, T. Kawano, R. Reifarth, et al., Phys. Rev. C **78**, 034609 (2008).

[22] S. F. Mughabghab, *Atlas of Neutron Resonances, 5$^{\text{th}}$ Edition* (Elsevier Science, 2006).

[23] J. M. Wouters, A. A. Vicente, T. A. Bredeweg, E. Esch, R. C. Haight, R. Hatarik, J. M. O'Donnell, R. Reifarth, R. S. Rundberg, J. M. Schwantes, et al., IEEE Trans. Nucl. Sci. **53**, 880 (2006).

[24] B. Million, A. Bracco, F. Camera, S. Brambilla, A. Gadea, D. Giugni, B. Herskind, M. Kmiecik, R. Isocrate, S. Leoni, et al., Nucl. Instrum. Methods A **452**, 422 (2000).

[25] R. Reifarth, T. A. Bredeweg, A. Alpizar-Vicente, J. C. Browne, E.-I. Esch, U. Greife, R. C. Haight, R. Hatarik, A. Kronenberg, J. M. O'Donnell, et al., Nucl. Instrum. Methods A **531**, 530 (2004).

[26] M. Jandel, Los Alamos National Laboratory, LA-UR-12-21171 (2012).

[27] A. Chyzh, B. Baramsai, J. A. Becker, F. Bečvář, T. A. Bredeweg, A. Couture, R. C. Haight, M. Jandel, J. Kroll, M. Krtička, et al., Phys. Rev. C **84**, 014306 (2011).

[28] B. Baramsai, G. E. Mitchell, U. Agvaanluvsan, F. Bečvář, T. A. Bredeweg, A. Chyzh, A. Couture, D. Dashdorj, R. C. Haight, M. Jandel, et al., Phys. Rev. C **85**, 024622 (2012).

[29] F. Bečvář, Nucl. Instrum. Methods A **417**, 434 (1998).

[30] T. von Egidy and D. Bucurescu, Phys. Rev. C **72**, 044311 (2005).

[31] Y. Kalmykov, T. Adachi, G. P. A. Berg, H. Fujita, K. Fujita, Y. Fujita, K. Hatanaka, J. Kamiya, K. Nakanishi, P. von Neumann-Cosel, et al., Phys. Rev. Lett. **96**, 012502 (2006).

[32] Y. Kalmykov, C. Özen, K. Langanke, G. Martínez-Pinedo, P. von Neumann-Cosel, and A. Richter, Phys. Rev. Lett. **99**, 202502 (2007).

[33] T. A. Brody, J. Flores, J. B. French, P. A. Mello, A. Pandey, and S. S. M. Wong, Rev. Mod. Phys. **53**, 385 (1981).

[34] C. E. Porter and R. G. Thomas, Phys. Rev. **104**, 483 (1956).

[35] G. Rusev, C. T. Angell, R. Beyer, F. Dönau, M. Erhard, E. Grosse, S. L. Hammond, A. L. Hutcheson, S. Frauendorf, A. R. Junghans, et al., AIP Conf. Proc. **1099**, 799 (2009).

[36] R. Massarczyk, R. Schwengner, F. Dönau, E. Litvinova, G. Rusev, R. Beyer, R. Hannaske, A. R. Junghans, M. Kempe, J. H. Kelley, et al., Phys. Rev. C **86**, 014319 (2012).

[37] G. Rusev, N. Tsoneva, F. Dönau, F. Frauendorf, R. Schwengner, A. P. Tonchev, A. S. Adekola, S. L. Hammond, J. H. Kelley, E. Kwan, et al., Phys. Rev. Lett. **110**, 022503 (2013).

[38] *Ripl-2, reference input parameter library*, URL `http://www-nds.iaea.org/ripl2/`.

[39] C. Kohstall, D. Belic, P. von Brentano, C. Fransen, A. Gade, R.-D. Herzberg, J. Jolie, U. Kneissl, A. Linnemann, A. Nord, et al., Phys. Rev. C **72**, 034302 (2005).

[40] V. A. Zheltonozhsky, V. M. Mazur, Z. M. Bigan, and D. M. Symochko, Bull. Russ. Acad. Sciences **72**, 1548 (2008).

[41] B. Bush and Y. Alhassid, Nucl. Phys. **A531**, 27 (1991).

[42] P. Möller, J. R. Nix, W. D. Myers, and W. J. Swiatecki, At. Data. Nucl. Data Tables **59**, 185 (1995).

[43] S. S. Dietrich and B. L. Berman, At. Data. Nucl. Data Tables **38**, 199 (1988).

[44] I. Bentley and S. Frauendorf, Phys. Rev. C **83**, 064322 (2011).

[45] S. G. Kadmenskii, V. P. Markushev, and V. I. Furman, Sov. J. Nucl. Phys. **37**, 165 (1983).

[46] A. B. Migdal, *Theory of finite Fermi systems, and applications to atomic nuclei* (Interscience Publishers, 1967).

[47] S. Agostinelli et al., Nucl. Instrum. Methods A **506**, 250 (2003).

[48] M. Jandel, T. A. Bredeweg, A. Couture, M. M. Fowler, E. M. Bond, M. B. Chadwick, R. R. C. Clement, E.-I. Esch, J. M. ODonnell, R. Reifarth, et al., Nucl. Instrum. Methods B **261**, 1117 (2007).

[49] M. Krtička (PhD dissertation, Charles University in Prague, 2002), URL `http://www-ucjf.troja.mff.cuni.cz/krticka/publikace/thesis.pdf`.